HAB79: A New Molecular Dataset for Benchmarking DFT and DFTB Electronic Couplings Against High-Level Ab-initio Calculations

Cite as: J. Chem. Phys. (in press) (2021); https://doi.org/10.1063/5.0076010
Submitted: 20 October 2021 • Accepted: 26 November 2021 • Accepted Manuscript Online: 27 November 2021

Orestis George Ziogos, Adam Kubas, Zdenek Futera, et al.

Accepted to J. Chem. Phys. 10.1063/5.0076010

HAB79: A New Molecular Dataset for Benchmarking DFT and DFTB Electronic Couplings Against High-Level Ab-initio Calculations

Orestis George Ziogos[1,a)], Adam Kubas[2], Zdenek Futera[3], Weiwei Xie[4], Marcus Elstner[4], and Jochen Blumberger[1,b)]

[1] Department of Physics and Astronomy and Thomas Young Centre, University College London, Gower Street, London WC1E 6BT, United Kingdom

[2] Institute of Physical Chemistry, Polish Academy of Sciences, Kasprzaka 44/52, 01-224 Warsaw, Poland

[3] Faculty of Science, University of South Bohemia, 370 05 Ceske Budejovice, Czech Republic

[4] Institute of Physical Chemistry, Karlsruhe Institute of Technology, 76131 Karlsruhe, Germany

[a)] Electronic mail: o.ziogos@ucl.ac.uk

[b)] Electronic mail: j.blumberger@ucl.ac.uk

Abstract

A new molecular dataset called HAB79 is introduced to provide ab-initio reference values for electronic couplings (transfer integrals) and to benchmark density functional theory (DFT) and density functional tight-binding (DFTB) calculations. The HAB79 dataset is comprised of 79 planar heterocyclic polyaromatic hydrocarbon molecules frequently encountered in organic (opto)electronics, arranged to 921 structurally diverse dimer configurations. We show that CASSCF/NEVPT2 with a minimal active space provides a robust reference method that can be applied to the relatively large molecules of the dataset. Electronic couplings are largest for cofacial dimers, in particular sulfur-containing polyaromatic hydrocarbons, with values in excess of 0.5 eV, followed by parallel displaced cofacial dimers. V-shaped dimer motifs, often encountered in the herringbone layers of organic crystals, exhibit medium-sized couplings whereas T-shaped dimers have the lowest couplings. DFT values obtained from the projector operator-based diabatization (POD) method are initially benchmarked against the smaller databases HAB11 (HAB7-) and found to systematically improve when climbing Jacob's ladder, giving mean relative unsigned errors (MRUE) of 27.7% (26.3%) for the GGA functional BLYP, 20.7% (15.8%) for hybrid functional B3LYP and 5.2% (7.5%) for the long-range corrected hybrid functional omega-

B97X. Cost effective POD in combination with a GGA functional (PBE) and very efficient DFTB calculations on the dimers of the HAB79 database give a good linear correlation with the CASSCF/NEVPT2 reference data, which, after scaling with a multiplicative constant, gives reasonably small MRUEs of 17.9% and 40.1%, respectively, bearing in mind that couplings in HAB79 vary over 4 orders of magnitude. The ab-initio reference data reported here are expected to be useful for benchmarking other DFT or semi-empirical approaches for electronic coupling calculations.

I. Introduction

One of the key parameters in molecular charge transport modeling and simulation is the electronic coupling between two diabatic charge transfer electronic states [1-4]. Electronic couplings (or charge transfer integrals) for a given molecular dimer configuration can be calculated using a variety of methods, including but not limited to ab-initio wavefunction, density functional theory (DFT), and semi-empirical or solely empirical methods [5-24]. The choice of a particular method is typically dictated by various factors, trying to strike a balance between chemical accuracy and computational resources utilization.

Although accurate ab-initio methods such as *n*-electron valence state perturbation theory NEVPT2 [25-27] and multi-reference configuration interaction [28] are considered a "golden standard" for charge transfer integral calculations, their practical implementation is hindered by their inherent complexity and the sheer amount of computational resources required in the case of extended systems or when a significant number of electronic coupling evaluations is needed. In order to overcome this obstacle, benchmark datasets are utilized as to evaluate the accuracy – and calibrate if needed – computationally less demanding methods [19, 21].

In this work, we introduce the HAB79 dataset: a selection of 79 heterocyclic polyaromatic hydrocarbons, either already utilized or inspired by contemporary organic (opto)electronic applications [29], arranged to 921 structurally diverse homomolecular dimers. Having such structural information at hand, ab-initio electronic couplings are calculated at the CASSCF/NEVPT2 level of theory, forming this way the HAB79 charge transfer integral reference dataset. DFT and density functional tight binding (DFTB) electronic couplings are calculated using the same dimeric configurations, thus enabling the direct comparison with reference ab-initio coupling values.

A general linear correlation between reference and DFT and DFTB electronic coupling values is identified, hence allowing the determination of a universal multiplicative

scaling constant for each method and level of theory that can be used for a-posteriori corrections. Furthermore, the HAB11 and HAB7- datasets from the literature are revisited by means of projection operator-based diabatization (POD) DFT electronic coupling calculations in order to examine the effect of various exchange-correlation functionals to the predictive capability of the POD method with respect to reference ab-initio data.

The layout of the paper is organized follows: all computational details regarding the construction of the HAB79 dataset and the employed simulation methods are outlined in Sec. II, followed by the results for all datasets in Sec. III. The conclusions of this work are presented in Sec. IV.

II. Computational details

II.1 HAB79 database

The HAB79 dataset is a compilation of planar heterocyclic polyaromatic hydrocarbons exhibiting either electron or hole conductivity, with N, O, F, and S heteroatoms significantly participating to the non-degenerate frontier molecular orbitals. This particular selection of molecules is based on either current or potential applications in the field or organic (opto)electronics [29-33]. The molecules of the HAB79 dataset are illustrated in Fig. 1, numbered in an ascending order with respect to the total number of electrons. A more comprehensive record of the HAB79 dataset including formal compound names and InChIKey values (where available) is listed in the supplementary material. The geometry of each molecule was optimized using DFT at the B3LYP/6-311g(d) [34, 35] level of theory as implemented in the NWChem package [36].

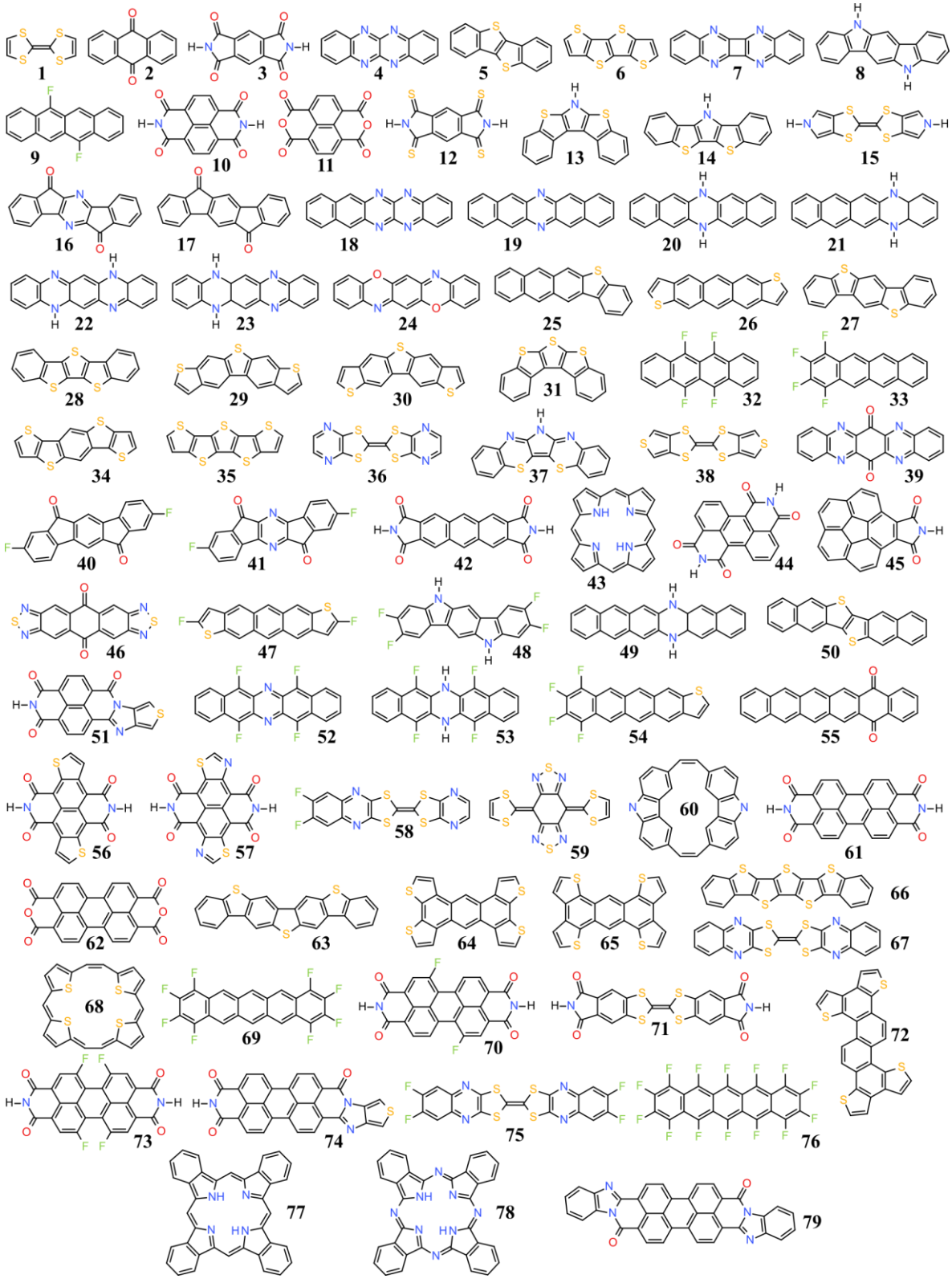

Fig. 1. The HAB79 molecular dataset.

Due to the planarity of all molecules in the dataset, one can define a local orthonormal system of coordinates for each molecule spanned by the normal vector to the conjugation

plane, $\vec{u}$, and two coplanar vectors, $\vec{c}_{\text{long}}$ and $\vec{c}_{\text{short}}$ with respect to the conjugation plane that characterize the long and short molecular axes according to the molecular mass distribution. These vectors are derived by the diagonalization of the molecular inertia tensor, thus retrieving the normal vector and short and long molecular axes vectors in an ascending order with respect to the sorted eigenvalue spectrum.

Such a local system of coordinates can be used to create a series of homo-molecular dimeric configurations. The simplest form is that of cofacial dimers: monomers are translated along $\vec{u}$ by a given distance, thus forming totally eclipsed structures, typically associated with high electronic couplings. Following prior work [19, 21], the distances of 3.5 Å, 4.0 Å, 4.5 Å, and 5.0 Å are chosen, resulting in four cofacial dimers per dataset entry. The next conformation of dimers under consideration are of the parallel-displaced (PD) type. A cofacial dimer with a vertical separation of 3.5 Å is initially created and is used to create three different PD dimers via appropriate translations along $\vec{c}_{\text{long}}$, $\vec{c}_{\text{short}}$, and $\vec{c}_{\text{long}} + \vec{c}_{\text{short}}$, respectively, as described in the supplementary material. Finally, a series of T-shaped dimers is created by means of proper displacements and rotations: as in the case of PD dimers, an initial cofacial dimer is created, followed by rigid body rotations of the second monomer about either $\vec{c}_{\text{long}}$ or $\vec{c}_{\text{short}}$ by 45° (also referred to as V-shaped) and 90°, making sure to alleviate any steric overlap by augmenting the vertical separation. Further information on T- and V-shaped dimers is included in the supplementary material. All dimer configurations are included in the supplementary material in xyz format.

II.2 Electronic coupling calculations

II.2.1 Ab-initio reference calculations

The reference couplings are obtained with the generalized Mulliken-Hush (GMH) approach [5, 37-43]. Within this method, the electronic coupling matrix element H_{ab} in a two-state donor-acceptor system is obtained from quantities calculated in an adiabatic (delocalized) basis using the following expression:

$$|H_{ab}| = \frac{|\mu_{12}|\Delta E_{12}}{\sqrt{(\mu_{11}-\mu_{22})^2+4(\mu_{12})^2}} \qquad (1)$$

where ΔE_{12} is a vertical excitation energy from the ground state 1 to the excited state 2, μ_{11} and μ_{22} denote the respective states' dipole moments, and μ_{12} is the transition dipole moment between the two states. In the case of symmetric dimers that possess a mirror plane perpendicular to the $\vec{u}$ vector, the Eq. (1) reduces to half the excitation energy ΔE_{12}.

The quantities that enter the Eq. (1) are calculated with the *n*-electron valence state perturbation theory (NEVPT2) [25-27] using state-averaged complete active space self-consistent field (CASSCF) reference wavefunction [44]. The averaging was over two doublet states for each dimer. Due to the size of the systems under study, the CASSCF active space was chosen as a minimal set comprising of two orbitals and three electrons (p-type carriers) or two orbitals and one electron (n-type carriers).

Our reference calculations utilize aug-cc-pVDZ basis set for heavy atoms and a smaller cc-pVDZ basis for hydrogen atoms [45, 46]. Such combination was shown to balance computational cost and accuracy for electronic coupling calculations [19]. The NEVPT2 calculations are carried out with an active "frozen core" approximation so that chemically inert core electrons are not correlated. The Coulomb and exchange integrals are efficiently evaluated with the resolution-of-identity (RI) [47, 48] and chain-of-spheres (COSX) approximations [49], respectively. The RI auxiliary basis set is aug-cc-pVDZ/C or cc-pVDZ/C [50]. The CASSCF/NEVPT2 calculations are performed with ORCA 4.2.0 package.

When comparing GMH results with outcomes from other methods, it is essential to ensure the couplings are calculated between the same donor-acceptor states. In the present case, we first generate a cube file with the natural molecular orbital (NMO) that is approximately singly occupied in the CASSCF ground state of a dimer. In the next step, we numerically compute its overlap with the cube file that contains grid data for the approximately singly occupied NMO obtained from the ground state, unrestricted DFT calculations that employ the PBE functional [51, 52]. The latter calculations are performed with the same setup as CASSCF, i.e. doublet electronic state, same basis functions and charge. An overlap close to unity confirms a similar nature of the CASSCF and DFT ground states. Subsequently, we screen computed CASSCF transition dipole moments for values lower than 0.1 D which allows us to identify states that are not of charge-transfer character but instead correspond to locally excited states. The final step involves visual inspection of CASSCF NMOs for cases where any of the two previous steps identified issues. Orbitals are then reordered, and the re-converged CASSCF wavefunction is checked against the two criteria. The overlap is calculated with Multiwfn 3.7 [53].

II.2.2 DFT approaches

Projection operator-based diabatization (POD). The POD method [10, 22, 24] is described in detail in Ref. [22] and we only briefly summarize the method here. First a Kohn-Sham calculation is carried out on the neutral dimer, unless stated otherwise, followed by

transformation of the KS Hamiltonian to a Löwdin-orthogonalized atomic orbital basis set. The resultant KS Hamiltonian is then rearranged in block form, with the first (second) block on the diagonal, $\widetilde{H}_{DD}$ ($\widetilde{H}_{AA}$), containing the orthogonal atomic orbitals centred on the donor (acceptor), $\widetilde{H} = \begin{bmatrix} \widetilde{H}_{DD} & \widetilde{H}_{DA} \\ \widetilde{H}_{AD} & \widetilde{H}_{AA} \end{bmatrix}$. The two blocks, $\widetilde{H}_{DD}$ and $\widetilde{H}_{AA}$, are diagonalized to $\bar{H} = \begin{bmatrix} \bar{H}_{DD} & \bar{H}_{DA} \\ \bar{H}_{AD} & \bar{H}_{AA} \end{bmatrix}$, where $\bar{H}_{DD}$ ($\bar{H}_{AA}$) are diagonal with diagonal elements $\epsilon_{D,i}$ ($\epsilon_{A,i}$). The corresponding orbitals are localized on the donor and acceptor molecules, respectively. The energy levels of neutral donor and neutral acceptor are filled with 2*N* electrons each (assuming that donor and acceptor have the same number of electrons). For hole transfer (electron transfer), the off-diagonal block element $[\bar{H}_{DA}]_{NN}$ ($[\bar{H}_{DA}]_{N+1N+1}$) is taken as the electronic coupling matrix element, i.e. the coupling between the diabatized HOMO (LUMO) orbitals of the donor and acceptor, respectively. Note that this procedure differs from the one we have previously employed, where calculations of coupling matrix elements were carried out on cationic (anionic) dimers. The current definition is the same as the one used in Ref. [24]. We found that both definitions give very similar results at POD/PBE level, though the definition used here is computationally more efficient.

POD calculations were first carried out on two smaller databases, HAB11 and HAB7- [19, 21] to test the performance of the exchange-correlation functional (XC) and basis set. We tested the PBE and BLYP generalized gradient approximation (GGA) XC functionals [34, 51, 52, 54], the PBE0 and B3LYP hybrid XC functionals [34, 35, 55], and HSE06, LRC-ωPBEh, and ωB97X range-separated hybrid XC functionals [56-58] and basis sets of variable size, namely DZVP-, TZVP- and TZV2P-GTH. POD calculations on the dimers of the HAB79 database were carried out at the PBE/DZVP-GTH level of theory [51, 52, 59]. All POD calculations were carried out with the CP2K package [60].

Electron transfer-fragment molecular orbital method (ET-FMO). Supplementary charge transfer integral calculations for the HAB79 dataset are carried out using the ET-FMO method [61] at the B3LYP/6-311g(d) level of theory, as implemented in NWChem. The ET-FMO method relies on the expression of one-electron dimer states using localized monomer molecular orbitals. Should the dimer HOMO-1 and HOMO (LUMO and LUMO+1) result from the interaction of monomer HOMOs (LUMOs) denoted as Ψ_i, the secular equation describing dimer orbital energies can be expressed as $HC - \epsilon SC = 0$, where $H = \begin{bmatrix} e_1 & J_{12} \\ J_{12} & e_2 \end{bmatrix}$ the Hamiltonian matrix and $S = \begin{bmatrix} 1 & S_{12} \\ S_{12} & 1 \end{bmatrix}$ the overlap matrix, with $e_i = \langle \Psi_i | \hat{H} | \Psi_i \rangle$ being

the site energy and $J_{ij} = \langle \Psi_i | \hat{H} | \Psi_j \rangle$ the transfer integral at the non-orthogonal frontier orbital basis set. Upon an appropriate Löwdin symmetric transformation, the Hamiltonian is expressed as $H^{\text{eff}} = \begin{bmatrix} e_1^{\text{eff}} & J_{12}^{\text{eff}} \\ J_{12}^{\text{eff}} & e_2^{\text{eff}} \end{bmatrix}$, with $J_{12}^{\text{eff}} = \frac{J_{12} - 0.5(e_1 + e_2)S_{12}}{1 - S_{12}^2}$ being the actual orthogonalized charge transfer integral.

II.2.3 DFTB approach

DFTB is derived from DFT by a Taylor expansion of the total energy around a well-defined reference density and is found to be 2−3 orders of magnitude faster than DFT-GGA functionals with midsized basis sets [62, 63]. Recent studies have shown that DFTB can provide electronic couplings in good agreement with other DFT approaches, and the application of a uniform scaling factor allows the accuracy comparable to high-level electronic-structure methods [19, 21]. In the present work, all calculations are performed within the framework of the fragment-orbital first-order DFTB (FODFTB1) with MIO parameter set [64]. Since charge transfer typically occurs in a narrow energy window around the Fermi level, we simplify the description of the charge by considering frontier orbitals of the fragments, i.e., HOMOs for hole transfer and LUMO for electron transfer.

III. Results and Discussion

III.1 Ab-initio electronic couplings for HAB79

The size of systems that enter the HAB79 database constitutes a challenge for high-level ab-initio calculations. In our previous study [19] we showed that MRCI+Q with large CASSCF active space provides results in excellent agreement with the full CI method. We also found a multireference perturbative approach such as NEVPT2 to provide couplings with a mean relative unsigned error of 6.9 % w.r.t. MRCI+Q. We also explored the CC2 method as an economical approach for larger systems and found that it has accuracy slightly lower than NEVPT2 [19, 21]. We note, however, that ROHF-based CC2 calculations have unfavorable scaling behavior with the system size, in particular when the calculations are performed without the use of symmetry.

The present manuscript explores an alternative route – NEVPT2 calculations with a minimal active space CASSCF reference wavefunction instead of a complete valence active orbital set. Such significant active space reduction compared to our previous study [19] is well justified owing to the nature of the systems under investigation. The geometries of the donor and acceptor molecules are identical, and the diabatic energies of the sites are either

equal (cofacial orientation) or only marginally different (PD and T-shaped dimers). We also note that the dimers selected to enter the HAB79 do not display pronounced multireference character. Moreover, the two orbitals that form the active space in each case always constitute a bonding and anti-bonding pair. Thus, the two-orbital space provides a balanced description of the two adiabatic states already at the CASSCF level, and small differential dynamic correlation contribution is well approximated with a NEVPT2 approach. Two additional elements of our protocol made the NEVPT2 calculations feasible on the entire HAB79 set: a compact aug-cc-pVDZ basis set and the frozen core approximation.

Table I compares electronic couplings obtained for the furane cofacial dimer calculated with four different set-ups. The NEVPT2 calculations in [19] did not explore frozen core approximation as it was not available at that time. This became possible with the newer ORCA versions, and when it is turned on, the agreement with MRCI+Q (by default carried out with frozen core) improves. Active space reduction from (11,10) to minimal (3,2) and reduction of basis set along with the release of symmetry restrictions did not deteriorate NEVPT2 couplings. These observations are further confirmed by calculations on two geometries of the dimer 1 – cofacial at an intermolecular separation of 4.0 Å and T-shaped structure (see Table II). Here, the active space reduction decreases the couplings by 2 meV (ca. 1 %) compared to the larger active space selected on the basis of occupation numbers of the unrestricted MP2 natural orbitals. Interestingly, the basis set incompleteness error of the aug-cc-pVDZ basis renders the couplings slightly too large compared to calculations with aug-cc-pVTZ. The impact is somehow smaller for cofacial dimers (error of 1 %) compared to T-shaped geometry (error of 4 %). In any case, our test calculations show that the use of a minimal active space along with diffuse, double-z basis set and frozen core approximation provides electronic couplings that are of benchmark quality for the HAB79 set.

Table I. Comparison of the electronic coupling matrix elements (expressed in meV) and the decay constant β for cofacial furane dimer (couplings calculated at four intermolecular distances) obtained with various ab-initio methods. The last column present results that were obtained with the set-up used throughout this study.

	MRCI+Q*	NEVPT2*	NEVPT2**	NEVPT2**
Basis set	aug-cc-pVTZ	aug-cc-pVTZ	aug-cc-pVTZ	aug-cc-pVDZ
Ref. CAS	(11,10)	(11,10)	(11,10)	(3,2)
Symmetry	C_{2v}	C_{2v}	C_{2v}	C_1
Frozen core	9 el.	off	9 el.	9 el.

d (Å)				
3.5	440.3	412.7	423.3	426.2
4.0	214.9	200.8	210.1	213.8
4.5	101.8	97.4	103.2	107.3
5.0	46.0	48.9	50.3	50.1
β (1/Å)	3.01	2.85	2.84	2.85

*: Ref. [19]

**: current work

Table II. Comparison of the electronic coupling matrix elements (expressed in meV) of the dimer 1 at two geometries computed at NEVPT2 level with active spaces of different size and with different basis sets.

Active space	Basis set	Cofacial (4.0 Å)	T-shape
(11,10)	aug-cc-pVDZ	251.1	188.9
(3,2)	aug-cc-pVDZ	249.2	186.7
	aug-cc-pVTZ	247.0	179.2

As regards dimers belonging to the HAB79 dataset, ab-initio electronic couplings span an interval from 0 to 500 meV in a near-contiguous manner. Cofacial dimers with a vertical separation of 3.5 Å exhibit the highest values, ranging from 300 to 500 meV, as expected due to augmented molecular orbital overlap and in-phase alignment. Cofacial dimeric configurations with separations of 4.0 and 4.5 Å populate the intervals between 150 and 250 meV and 50 and 150 meV, respectively. Finally, cofacial dimers with a core distance of 5.0 Å are restricted to electronic coupling values below 50 meV.

In an attempt to classify all HAB79 dataset molecules regarding their potential charge transfer capabilities, one can examine the relationship between the electronic coupling of a given dimeric configuration and the single molecule reorganization energy λ [3, 65, 66]. If the coupling value is larger than $\lambda/2$, then no activation barrier for electron transfer exists (assuming zero driving force) and, as a consequence, the charge delocalizes over donor and acceptor. If this configuration is periodically replicated in a crystal the charge transport is likely to occur via (fast) diffusion of a delocalized polaron, unless structural defects or other charge localizing effects are present. We simply refer to this case as “band-like” mechanism. In the opposite regime, if the coupling is smaller than $\lambda/2$, an activation barrier for electron transfer exists and the mechanism would be (slow) hopping of a relatively localized polaron.

Having this categorization in mind, all cofacial dimers with a separation of 3.5 Å and the majority of 4.0 Å dimers clearly lie in the band-like charge transfer regime, as illustrated in Fig. 2.

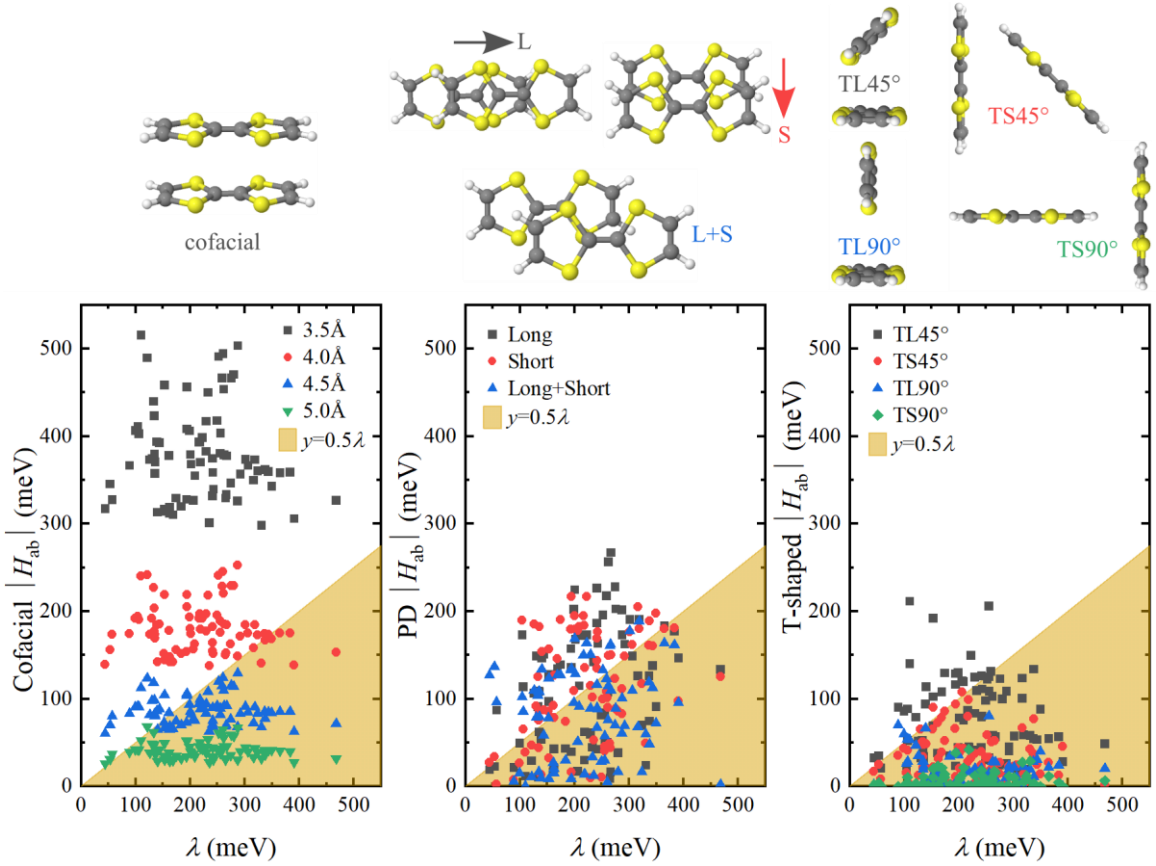

Fig. 2. Correlation diagrams between reorganization energy and ab-initio electronic couplings for all HAB79 dimers. Dimers in the area depicted in yellow support stable localized (diabatic) electronic states resulting in hopping transport. Dimers outside this area do not support stable localized electronic states resulting in delocalized or band-like polaronic transport when periodically replicated. Left panel is for cofacial dimers, middle panel for parallel displaced (PD) dimers where displacement is along the short, long or diagonal (short+long) axis, and right panel is for T-shaped dimers with rotation about the long (TL) or short axis (TS). Dimer configurations based on tetrathiafulvalene are also included as to illustrate the different intermolecular arrangements, with the vectors annotated as "L" and "S" corresponding to the long and short molecular axes vectors, respectively.

The highest electronic coupling values for 3.5 Å cofacial dimers are reported for sulfur-containing PAHs: dibenzo[b,b']thieno[2,3-f:5,4-f']bis[1]benzothiophene (DBTBT; molecule **63**) and tetrathiafulvalene (TTF; molecule **1**) register coupling values of 515 and

503 meV, respectively, closely followed by compounds **12**, **27**, and **38** [67-71]. Of particular importance is also the case of nitrogen-based macrocycles like pristine and benzo-annulated porphyrin (**43** and **77**), and phthalocyanine (**78**) [72, 73]: due to their low reorganization energy values, cofacial dimers of such molecules appear to lie in the band-like charge transfer regime – even for large core separations.

In the case of PD dimers, electronic couplings are limited to below 300 meV, with the highest values associated with perylene derivatives (compounds **61**, **62**, and **70**) and fully (**76**) and partially (**69**) fluorinated pentacene [30, 74-76], all situated in the band-like charge transfer regime. If one applies the $\lambda/2$ categorization criterion, PD dimers of all three types (i.e. displaced along the long, short, and composite directions) can be found in the band-like conductivity mechanism regime.

The third broad dimer category corresponds to T-shaped dimers. Electronic couplings for such dimeric configurations are limited to around 200 meV, with the largest values belonging to DBTBT (**63**) and V-shaped thienobisbenzothiophenes **29** and **30** [77, 78]. In contrast to cofacial and PD dimer configurations, T-shaped dimers belonging to the band-like charge transfer regime are limited to rotations about the long axis by 45º, although there exist some cases on the $\lambda/2$ dividing line, for 45º rotations about the short axis, primarily for nitrogen-containing rod-like molecules (**4**, **7**, **18**, **19**, **21**, **23**, **39**) and partially fluorinated tetracenes (**9** and **32**) [32, 79, 80].

III.2 DFT POD electronic couplings for HAB11 and HAB7-

Ab-initio calculated electronic couplings from the HAB79 dataset are used as reference in order to evaluate the suitability of computationally less intensive methods, namely DFT and DFTB approaches. Before we present the DFT POD results for HAB79, we investigate the performance of different XC functionals and basis sets on two smaller databases of pi-conjugated organic homo-dimers for which similar ab-initio reference data are available, HAB11 and HAB7- [19, 21].

A suitable metric of the correlation between electronic coupling values obtained using a specific calculation method and the reference dataset is the inverse of the slope coefficient derived by means of a linear least squares regression fitting procedure, corresponding to the linear scaling constant. Further quantitative assessments are carried out using a series of statistical error metrics, such as the mean unsigned error (MUE) $\mathrm{MUE} = \sum_n |y_{\mathrm{calc}} - y_{\mathrm{ref}}|/n$, the mean relative unsigned and signed errors (MRUE and MRSE, respectively) MRUE =

$\sum_n(|y_{\text{calc}} - y_{\text{ref}}|/y_{\text{ref}})/n$ and MRSE $= \sum_n(y_{\text{calc}}/y_{\text{ref}} - 1)/n$, and the maximum unsigned error (MAX) MAX $= \max|y_{\text{calc}} - y_{\text{ref}}|$.

Electronic couplings from cofacial dimer configurations are further utilized for the calculation of the exponential distance decay constant β satisfying the equation $|H_{\text{ab}}| = A\exp(-0.5\beta d)$, where d is the vertical separation between monomers. Furthermore, all aforementioned error estimates are also applied to the derived exponential decay constant values.

Scaling constants and statistical error metrics for the HAB7- and HAB11 datasets are listed in Table III and Table IV. Due to the larger size of molecules belonging to the HAB7- dataset, DFT calculations were restricted to DZVP and TZVP basis sets, whereas for the smaller molecules of the HAB11 dataset, the TZV2P basis set was used. Discrepancies with previously reported values on the HAB11 dataset are due to differences in dimer charge and an erroneous definition of the PBE0 XC functional in Ref. [22] which is here corrected.

Table III. Linear scaling constants between reference and DFT POD couplings and error statistics on electronic couplings and exponential decay parameters β for the HAB7- dataset for different XC functionals using a TZVP-GTH basis set. Values in parentheses correspond to DFT calculations using a DZVP-GTH basis set. Scaled PBE (sPBE) correspond to DZVP-GTH/PBE values multiplied by 1.325.

XC	PBE	PBE0	HSE06	LRC-ωPBEh	BLYP	B3LYP	ωB97X	sPBE
Scaling const.	1.368 (1.325)	1.200 (1.157)	1.203 (1.161)	1.139	1.355	1.214	1.030	1.000
MUE $\|H_{\text{ab}}\|$ (meV)	49.1 (45.2)	29.9 (24.8)	30.5 (25.5)	21.2	47.5	31.0	8.3	6.2
MRUE $\|H_{\text{ab}}\|$ (%)	27.4 (25.4)	15.5 (13.5)	16.0 (14.0)	10.4	26.3	15.8	7.5	5.4
MRSE $\|H_{\text{ab}}\|$ (%)	-27.4 (-25.4)	-15.5 (-12.3)	-16.0 (-13.1)	-8.9	-26.3	-15.8	4.8	-1.1
MAX $\|H_{\text{ab}}\|$ (meV)	110.6 (98.8)	72.6 (56.0)	73.0 (56.6)	55.4	108.7	77.3	30.9	20.5
MUE β (Å^{-1})	0.13 (0.12)	0.13 (0.12)	0.13 (0.12)	0.15	0.13	0.14	0.27	0.12
MRUE β (%)	4.4 (4.1)	4.4 (4.2)	4.4 (4.0)	5.0	4.4	4.7	9.0	4.1
MRSE β (%)	1.1 (1.6)	-1.1 (-1.2)	-0.6 (-0.5)	-3.5	-0.1	-2.6	-9.0	1.6
MAX β (Å^{-1})	0.25 (0.25)	0.23 (0.24)	0.22 (0.22)	0.29	0.21	0.26	0.44	0.25

Table IV. Linear scaling constant between reference and DFT POD couplings and error statistics on electronic couplings and exponential decay parameters β for the HAB11 dataset for different XC functionals using a TZV2P-GTH basis set. Scaled PBE (sPBE) correspond to PBE values multiplied by 1.395.

XC	PBE	PBE0	HSE06	LRC-ωPBEh	BLYP	B3LYP	ωB97X	sPBE
Scaling const.	1.395	1.254	1.262	1.163	1.383	1.263	1.066	1.000
MUE $\lvert H_{ab}\rvert$ (meV)	60.8	44.0	45.3	29.5	58.7	44.1	12.2	6.1
MRUE $\lvert H_{ab}\rvert$ (%)	29.2	21.5	22.4	13.5	27.7	20.7	5.2	3.6
MRSE $\lvert H_{ab}\rvert$ (%)	-29.2	-21.5	-22.4	-13.5	-27.7	-20.7	-4.3	-1.2
MAX $\lvert H_{ab}\rvert$ (meV)	147.5	108.0	110.2	78.1	145.7	115.1	48.6	22.6
MUE β ($Å^{-1}$)	0.07	0.08	0.09	0.06	0.07	0.06	0.06	0.07
MRUE β (%)	2.6	2.8	3.0	2.0	2.4	2.2	2.2	2.6
MRSE β (%)	0.7	1.4	2.0	-1.1	-0.4	-0.4	-1.9	0.7
MAX β ($Å^{-1}$)	0.14	0.13	0.15	0.16	0.14	0.14	0.17	0.14

For both HAB7- and HAB11 datasets, statistical measures, such as the MUE and MRUE for DFT POD electronic couplings, exhibit an almost systematic improvement from GGA XC functionals to global hybrids (PBE0, B3LYP) to long-range (LR) corrected hybrid XC functionals, with ωB97X exhibiting the best performance and a scaling factor very close to unity. As regards PBE-based XC functionals, the transition from the global hybrid PBE0 to the short-range corrected HSE06 functional is linked with no actual improvement. In the case of the exponential distance decay constants, ab-initio reference values are well reproduced by GGA XC functionals, with the presence of Hartree-Fock exchange (HFX) in the LR region leading to slower decay.

This behavior is typical for POD where the charge density is optimized on the whole dimer and the HFX in LR enhances the overlap between the monomer densities in the intermolecular region due to an improved description of the asymptotic behaviour of the XC potential. This is in contrast to electronic couplings obtained from constrained density functional theory (CDFT) [9, 15], which are generally too high with GGA XC and decrease to values in good agreement with ab-initio reference data upon inclusion of HFX [15, 19, 21 81-83]. The reason is that in CDFT the charge constrained states are optimized for charged donor-acceptor pairs and these states are still subject to the electron delocalization error, albeit to a lesser extent than adiabatic electronic states. For GGA XC the delocalization of the charge constrained states leads to too large overlaps and couplings, and this situation drastically improves when HFX functionals are used.

Finally, the effect of basis set size to the electronic couplings error statistics for the HAB7- dataset indicate that the utilization of a smaller basis set such as DZVP-GTH has a minimal effect. As a result, an alternative to using computationally demanding levels of theory, such as TZVP-GTH/ωB97X, is to calculate electronic couplings using a GGA XC functional and the small DZVP-GTH basis set and apply an a-posteriori scaling of the results by an appropriate multiplicative constant. As we show in the following, this approach can give very accurate numbers and at the same time allows for a very large number of coupling calculations, which could be beneficial in computational screening studies.

III.3 DFT POD, ET-FMO and DFTB electronic couplings for HAB79

DFT- and DFTB-based calculations under study exhibit strong linear correlations, both in comparison with the reference data and between them, as illustrated in the diagrams in Fig. 3. Moreover, the statistical distribution of the exponential distance decay constants for reference and DFT and DFTB calculations are depicted in Fig. 4.

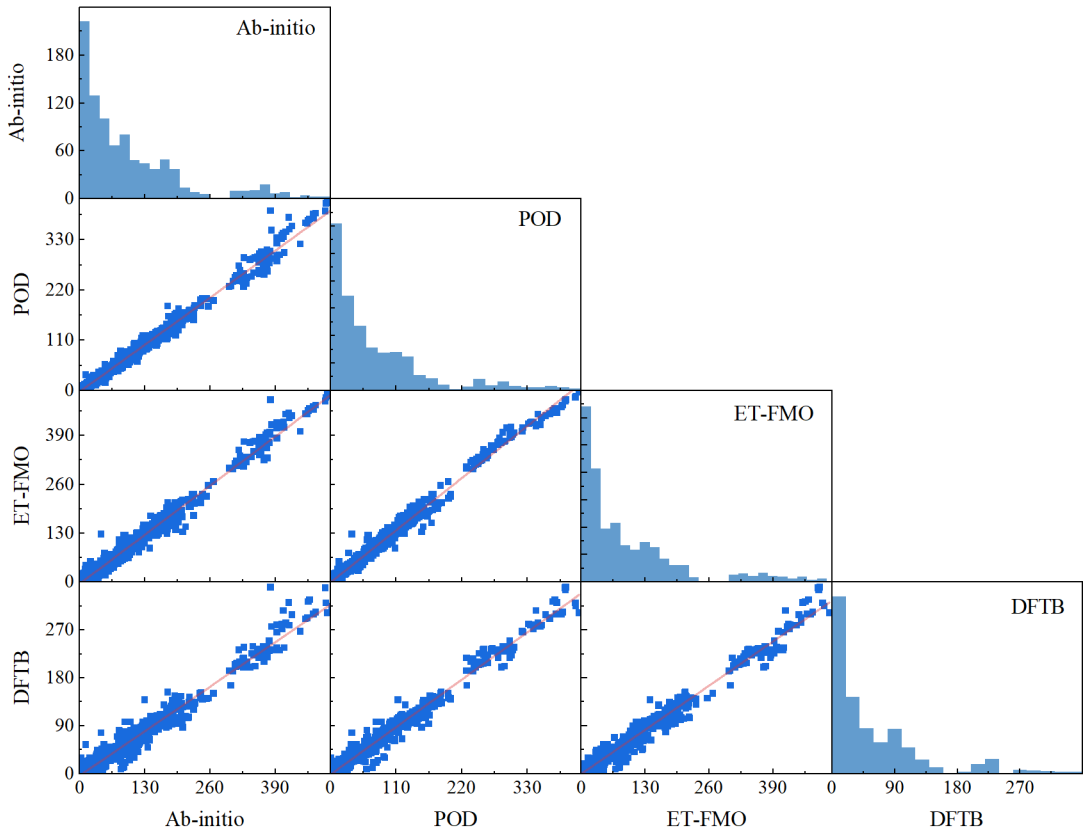

Fig. 3. Electronic couplings correlation diagrams and statistical distributions for the HAB79 dataset. All coupling values are expressed in meV.

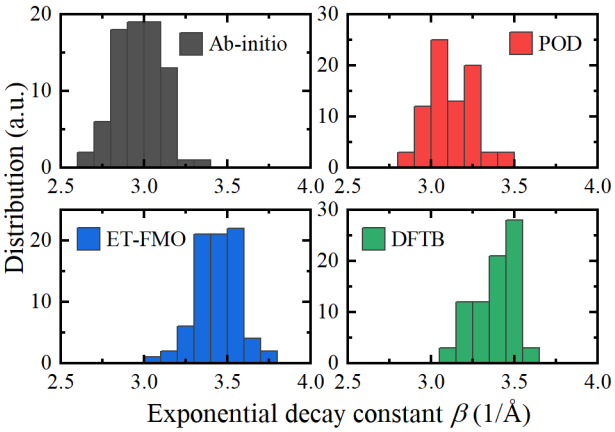

Fig. 4. Statistical distributions of the exponential decay constant β for cofacial dimers of the HAB79 dataset.

Scaling constants and statistical error metrics for the HAB79 dataset are listed in Table V. All electronic couplings error statistical metrics are also recalculated using the linear scaling constants, resulting in significant statistical improvements regarding the POD and DFTB calculations.

Table V. Linear scaling constants between reference and DFT and DFTB couplings and error statistics on electronic couplings and exponential decay parameters β for the HAB79 dataset. Values obtained after scaling are given in parentheses.

Method	POD	ET-FMO	DFTB
Scaling const.	1.282	1.017	1.600
MUE $\lvert H_{ab}\rvert$ (meV)	24.3 (8.5)	10.8 (10.8)	41.5 (14.5)
MRUE $\lvert H_{ab}\rvert$ (%)	29.8 (17.9)	28.2 (28.2)	52.4 (40.1)
MRSE $\lvert H_{ab}\rvert$ (%)	-24.6 (-3.3)	-1.5 (0.2)	-33.8 (5.9)
MAX $\lvert H_{ab}\rvert$ (meV)	122.0 (125.0)	104.9 (113.3)	191.8 (179.9)
MUE β (Å^{-1})	0.16	0.48	0.42
MRUE β (%)	5.4	16.2	14.3
MRSE β (%)	5.4	16.2	14.2
MAX β (Å^{-1})	0.37	0.66	0.81

The ET-FMO DFT method at the B3LYP/6-311g(d) level of theory exhibits the best correlation with respect to the reference ab-initio data (slope closest to 1). However, given its performance on the HAB7- and HAB11 database, we expect POD to exhibit a similarly good correlation as ET-FMO if POD had been carried out with a hybrid functional. Importantly, both methods have a very similar MRUE, but the one for POD can be significantly reduced by applying a multiplicative scaling factor of 1.282 upon which the MRUE decreases from 29.8 to 17.9%. DFTB-based couplings require a scaling by 1.6 and are associated with the largest error metric values. Nevertheless, upon scaling, the error metrics decreases. The larger value of the DFTB scaling factor compared to the DFT methods is due to the minimal basis set utilized for the calculation of DFTB electronic couplings. Similar scaling factors have been reported for datasets in the literature, namely 1.795 for the HAB7- dataset and 1.54 for the HAB11 dataset [19, 21].

As regards the errors in the exponential distance decay constant β, the POD method features the lowest values, with a MUE of 0.16 $Å^{-1}$ and a MRSE of 5.4%, whereas the other two methods exhibit larger statistical errors. A similar picture of the effect of the electronic coupling calculation method on the exponential decay constants is visible in the histograms in Fig. 4, where the shifting of the distributions towards larger β values upon selecting POD, ET-FMO, and DFTB calculations is evident.

A more in-depth analysis of the electronic couplings correlations between ab-initio reference values and DFT and DFTB results is carried out by examining the data according to the carrier type (p-type and n-type for hole and electron conductors, respectively) and the dimer type. This breakdown of the original set of electronic couplings data for the HAB79 dataset is illustrated for p-type molecules in Fig. 5 and n-type molecules in Fig. 6.

Accepted to J. Chem. Phys. 10.1063/5.0076010

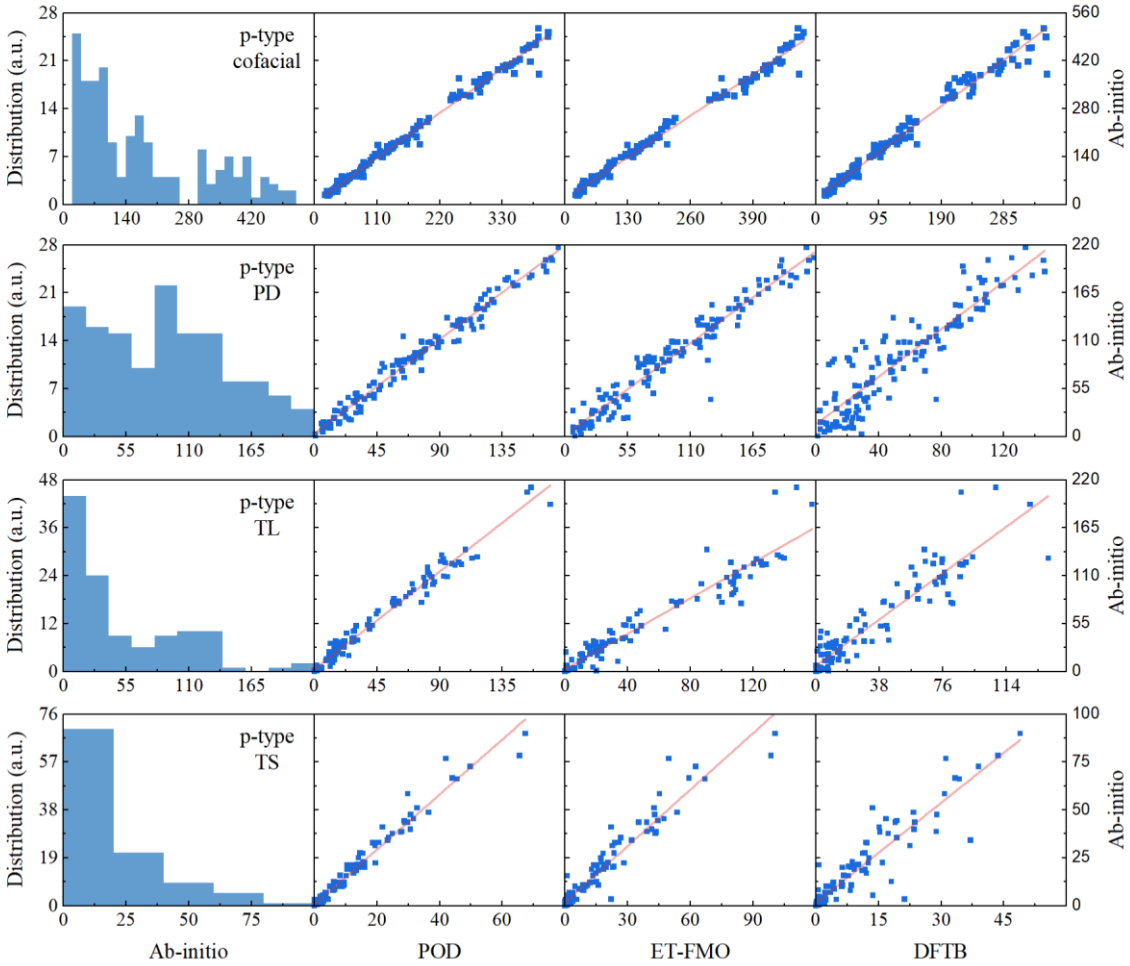

Fig. 5. Electronic couplings decomposition diagrams per dimer type for hole conducting molecules of the HAB79 dataset.

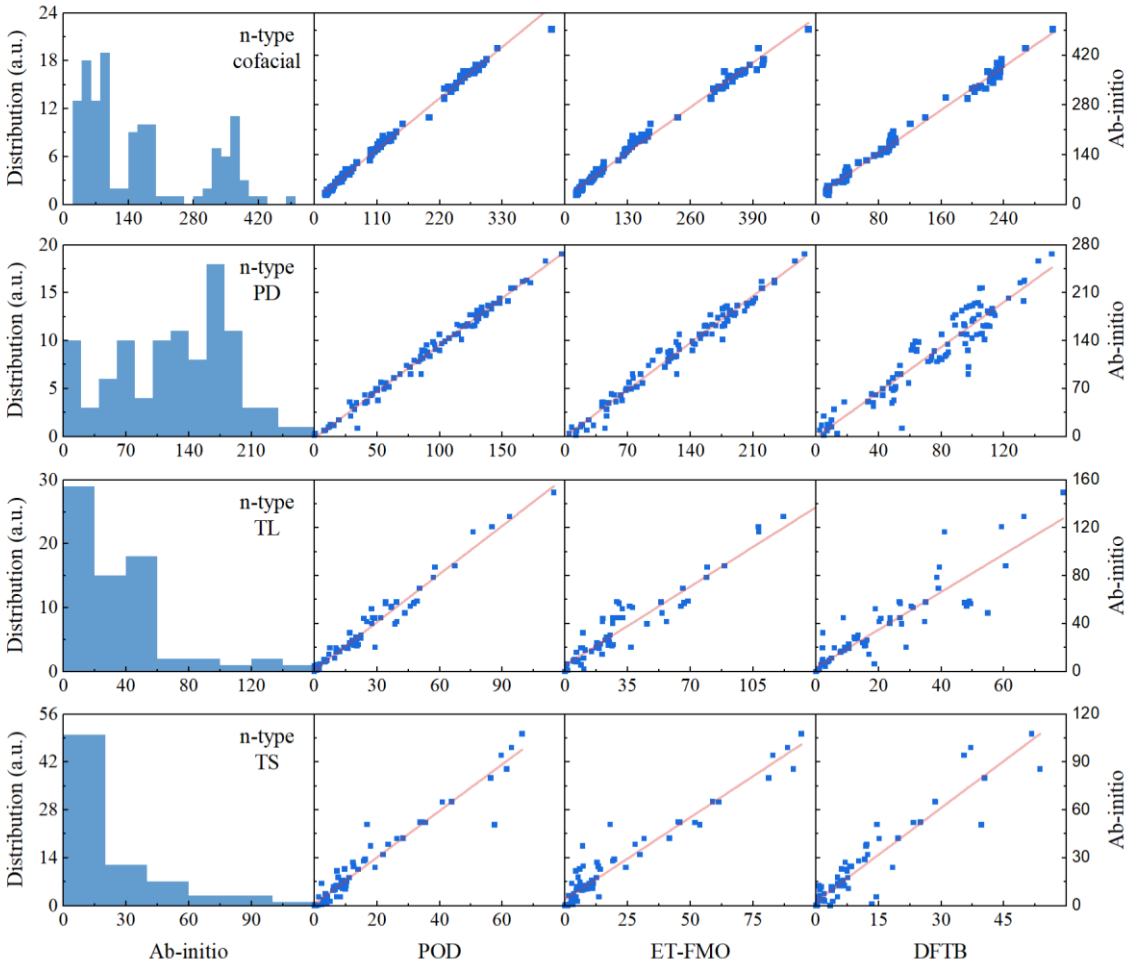

Fig. 6. Electronic couplings decomposition diagrams per dimer type for electron conducting molecules of the HAB79 dataset.

A general linear correlation with respect to the reference data for both carrier types and all four dimer types is evident. Moreover, error statistics as reported in the supplementary material indicate that following a multiplicative scaling according to Table V, metrics such as the MUE and MRSE are improved in a similar manner, regardless of carrier or dimer type.

IV. Conclusions

In this work, the HAB79 molecular dataset for benchmarking intermolecular electronic couplings is introduced, featuring 79 single molecules and 921 diverse dimeric configurations. For every dimer in the HAB79 dataset, we calculate ab-initio electronic couplings by means of the GMH method at a validated, minimal active space CASSCF/NEVPT2 level of theory, thus forming a reference charge transfer integral dataset in order to benchmark DFT and DFTB electronic coupling calculation schemes.

DFT-based couplings using the POD method at the PBE/DZVP-GTH level of theory show an excellent linear correlation with respect to reference ab-initio values, best described by a multiplicative scaling constant of 1.282. Upon applying such a scaling, the MRSE is significantly improved from -24.6% to -3.3%, hence constituting a-posteriori scaled PBE/DZVP-GTH POD electronic coupling calculations a relatively straightforward method of choice, with augmented predictive capabilities at a reasonable computational cost. If the POD method is used in combination with computationally more expensive functionals, e.g. range-separated hybrids, the error reduces significantly to MRSEs of about 5% for HAB11 and HAB7- (without scaling). Furthermore, DFT couplings by means of the ET-FMO method using the widely popular B3LYP XC functional and a 6-311g(d) triple-zeta all-electron basis set exhibit a fine correlation with reference data. The most cost-effective method in this work as regards computational resources utilizes DFTB calculations, with a linear scaling constant of 1.600 which improves the MRSE from -33.8% to 5.9%.

Regarding possible structure-property relationships arising from a direct comparison between HAB79 electronic couplings and reorganization energy, most cofacial dimers up to a separation of 4.0 Å can potentially manifest band-like charge transport characteristics – if such motifs are periodically replicated in a molecular crystal. In the case of PD dimers, some systems fall into the aforementioned transport regime, whereas for T-shaped dimers, such a behavior is only evident for selected dimers with a rotation of 45° about the short molecular axis.

The HAB7- and HAB11 datasets are revisited using POD charge transfer integral calculations with a variety of XC functionals. All functionals tend to capture the exponential decay constant β for cofacial dimers very well, but pure GGA XC exhibit too low absolute coupling values. The agreement with ab-initio couplings improves considerably for hybrids and range-separated hybrids. The optimal level of theory with respect to POD electronic coupling error minimization is based on the LR-corrected hybrid ωB97X XC functional and a triple-zeta basis set, giving MRUEs of 5.2% and 7.5% for HAB11 and HAB7- databases, respectively (without scaling).

We anticipate the newly introduced HAB79 dataset to provide useful ab-initio reference electronic coupling values to the computational charge transport community, enabling further benchmark work using various computational methodologies not covered by this work.

Supplementary material

Refer to the supplementary material for an extended record of the HAB79 including IUPAC or compound names, InChIKey values (where available), chemical formulae, carrier type, total number of electrons, frontier orbital energy levels, and reorganization energies, details regarding dimer geometric constructions, error statistics for the HAB79 dataset per carrier and dimer type, and POD electronic coupling and exponential decay parameters for the HAB7- and HAB11 datasets. HAB79 dimer geometries are also included in xyz format and all electronic coupling values are included in JSON file format.

Acknowledgments

This work was supported by the European Research Council (ERC) under the European Union Horizon 2020 research and innovation program (Grant Agreement No. 682539/ SOFTCHARGE). Via our membership of the UK's HEC Materials Chemistry Consortium, which is funded by EPSRC (Grant Nos. EP/L000202 and EP/R029431), this work used the ARCHER UK National Supercomputing Service (http://www.archer.ac.uk), as well as the UK Materials and Molecular Modeling (MMM) Hub, which is partially funded by EPSRC (Grant No. EP/P020194), for computational resources. The authors also acknowledge the use of UCL Grace and Kathleen High Performance Computing Facilities. AK acknowledges support from the National Science Centre, Poland, grant number 2018/30/E/ST4/00004 and access to high performance computing resources provided by the Interdisciplinary Centre for Mathematical and Computational Modelling in Warsaw, Poland, under grant GB79-5. WX acknowledges support by the Virtual Material Design (VirtMat) program and access to computing resources provided by InstitutsCluster II (Karlsruhe).

Data availability

The data that support the findings of this study are available from the corresponding author upon reasonable request.

References

[1] R. A. Marcus, J. Chem. Phys. **24**, 966 (1956).

[2] M. D. Newton, Chem. Rev. **91**, 767 (1991).

[3] H. Oberhofer, K. Reuter, and J. Blumberger, Chem. Rev. **117**, 10319 (2017).

[4] G. Gryn'ova, K.-H. Lin, and C. Corminboeuf, J. Am. Chem. Soc. **140**, 16370 (2018).

[5] R. J. Cave and M. D. Newton, J. Chem. Phys. **106**, 9213 (1997).

[6] A. A. Voityuk and N. Rösch, J. Chem. Phys. **117**, 5607 (2002).

[7] K. Senthilkumar, F. C. Grozema, F. M. Bickelhaupt, and L. D. A. Siebbeles, J. Chem. Phys. **119**, 9809 (2003).

[8] A. Migliore, S. Corni, R. D. Felice, and E. Molinari, J. Chem. Phys. **124**, 064501 (2006).

[9] Q. Wu and T. V. Voorhis, J. Chem. Phys. **125**, 164105 (2006).

[10] I. Kondov, M. Čížek, C. Benesch, H. Wang, and M. Thoss, J. Phys. Chem. C **111**, 11970 (2007).

[11] C.-P. Hsu, Z.-Q. You, and H.-C. Chen, J. Phys. Chem. C **112**, 1204 (2008).

[12] A. Migliore, P. H.-L. Sit, and M. L. Klein, J. Chem. Theory Comput. **5**, 307 (2009).

[13] T. Kubař and M. Elstner, J. Phys. Chem. B **114**, 11221 (2010).

[14] A. de la Lande and D. R. Salahub, J. Mol. Struct. THEOCHEM **943**, 115 (2010).

[15] H. Oberhofer and J. Blumberger, J. Chem. Phys. **133**, 244105 (2010).

[16] H. Oberhofer and J. Blumberger, Angew. Chem. - Int. Ed. **49**, 3631 (2010).

[17] M. Pavanello, T. V. Voorhis, L. Visscher, and J. Neugebauer, J. Chem. Phys. **138**, 054101 (2013).

[18] F. Gajdos, S. Valner, F. Hoffmann, J. Spencer, M. Breuer, A. Kubas, M. Dupuis, and J. Blumberger, J. Chem. Theory Comput. **10**, 4653 (2014).

[19] A. Kubas, F. Hoffmann, A. Heck, H. Oberhofer, M. Elstner, and J. Blumberger, J. Chem. Phys. **140**, 104105 (2014).

[20] P. Ramos, M. Papadakis, and M. Pavanello, J. Phys. Chem. B **119**, 7541 (2015).

[21] A. Kubas, F. Gajdos, A. Heck, H. Oberhofer, M. Elstner, and J. Blumberger, Phys. Chem. Chem. Phys. **17**, 14342 (2015).

[22] Z. Futera and J. Blumberger, J. Phys. Chem. C **121**, 19677 (2017).

[23] D. Manna, J. Blumberger, J. M. L. Martin, and L. Kronik, Mol. Phys. **116**, 2497 (2018).

[24] S. Ghan, C. Kunkel, K. Reuter, and H. Oberhofer, J. Chem. Theory Comput. **16**, 7431 (2020).

[25] C. Angeli, R. Cimiraglia, S. Evangelisti, T. Leininger, and J.-P. Malrieu, J. Chem. Phys. **114**, 10252 (2001).

[26] C. Angeli, R. Cimiraglia, and J.-P. Malrieu, Chem. Phys. Lett. **350**, 297 (2001).

[27] C. Angeli, R. Cimiraglia, and J.-P. Malrieu, J. Chem. Phys. **117**, 9138 (2002).

[28] P. G. Szalay, T. Müller, G. Gidofalvi, H. Lischka, and R. Shepard, Chem. Rev. **112**, 108 (2011).

[29] C. Wang, H. Dong, W. Hu, Y. Liu, and D. Zhu, Chem. Rev. **112**, 2208 (2011).

[30] J. Dhar, U. Salzner, and S. Patil, J Mater. Chem. C **5**, 7404 (2017).

[31] J. T. E. Quinn, J. Zhu, X. Li, J. Wang, and Y. Li, J. Mater. Chem. C **5**, 8654 (2017).

[32] A. N. Lakshminarayana, A. Ong, and C. Chi, J. Mater. Chem. C **6**, 3551 (2018).

[33] A. Venkateswararao, S.-W. Liu, and K.-T. Wong, Mater. Sci. Eng. R Rep. **124**, 1 (2018).

[34] C. Lee, W. Yang, and R. G. Parr, Phys. Rev. B **37**, 785 (1988).

[35] A. D. Becke, J. Chem. Phys. **98**, 5648 (1993).

[36] E. Aprà, E. J. Bylaska, W. A. de Jong, N. Govind, K. Kowalski, T. P. Straatsma, M. Valiev, H. J. J. van Dam, Y. Alexeev, J. Anchell, V. Anisimov, F. W. Aquino, R. Atta-Fynn, J. Autschbach, N. P. Bauman, J. C. Becca, D. E. Bernholdt, K. Bhaskaran-Nair, S. Bogatko, P. Borowski, J. Boschen, J. Brabec, A. Bruner, E. Cauët, Y. Chen, G. N. Chuev, C. J. Cramer, J. Daily, M. J. O. Deegan, T. H. Dunning, M. Dupuis, K. G. Dyall, G. I. Fann, S. A. Fischer, A. Fonari, H. Früchtl, L. Gagliardi, J. Garza, N. Gawande, S. Ghosh, K. Glaesemann, A. W. Götz, J. Hammond, V. Helms, E. D. Hermes, K. Hirao, S. Hirata, M. Jacquelin, L. Jensen, B. G. Johnson, H. Jónsson, R. A. Kendall, M. Klemm, R. Kobayashi, V. Konkov, S. Krishnamoorthy, M. Krishnan, Z. Lin, R. D. Lins, R. J. Littlefield, A. J. Logsdail, K. Lopata, W. Ma, A. V. Marenich, J. M. del Campo, D. Mejia-Rodriguez, J. E. Moore, J. M. Mullin, T. Nakajima, D. R. Nascimento, J. A. Nichols, P. J. Nichols, J. Nieplocha, A. Otero-de-la-Roza, B. Palmer, A. Panyala, T. Pirojsirikul, B. Peng, R. Peverati, J. Pittner, L. Pollack, R. M. Richard, P. Sadayappan, G. C. Schatz, W. A. Shelton, D. W. Silverstein, D. M. A. Smith, T. A. Soares, D. Song, M. Swart, H. L. Taylor, G. S. Thomas, V. Tipparaju, D. G. Truhlar, K. Tsemekhman, T. V. Voorhis, Á. Vázquez-Mayagoitia, P. Verma, O. Villa, A. Vishnu, K. D. Vogiatzis, D. Wang, J. H. Weare, M. J. Williamson, T. L. Windus, K. Woliński, A. T. Wong, Q. Wu, C. Yang, Q. Yu, M. Zacharias, Z. Zhang, Y. Zhao, and R. J. Harrison, J. Chem. Phys. **152**, 184102 (2020).

[37] R. J. Cave and M. D. Newton, Chem. Phys. Lett. **249**, 15 (1996).

[38] R. S. Mulliken, J. Am. Chem. Soc. **74**, 811 (1952).

[39] R. S. Mulliken and W. B. Person, Molecular Complexes (Wiley, New York, 1969).

[40] N. S. Hush, Prog. Inorg. Chem. **8**, 391 (1967).

[41] N. S. Hush, Electrochim. Acta **13**, 1005 (1968).

[42] J. R. Reimers and N. S. Hush, J. Phys. Chem. **95**, 9773 (1991).

[43] C. Creutz, M. D. Newton, and N. Sutin, J. Photochem. Photobiol. A **82**, 47 (1994).

[44] B. O. Roos, P. R. Taylor and P. E. M. Sigbahn, Chem. Phys. **48**, 157 (1980).

[45] T. H. Dunning Jr., J. Chem. Phys. **90**, 1007 (1989).

[46] D. E. Woon and T. H. Dunning Jr., J. Chem. Phys. **98**, 1358 (1993).

[47] K. Eichkorn, O. Treutler, H. Ohm, M. Häser, and R. Ahlrichs, Chem. Phys. Lett. **240**, 283 (1995).

[48] M. Sierka, A. Hogekamp, and R. Ahlrichs, J. Chem. Phys. **118**, 9136 (2003).

[49] R. Izsák, and F. Neese, J. Chem. Phys. **135**, 144105 (2011).

[50] F. Weigend, A. Kohn, C. Hattig, J. Chem. Phys. **116**, 3175 (2002).

[51] J. P. Perdew, K. Burke, and M. Ernzerhof, Phys. Rev. Lett. **77**, 3865 (1996).

[52] J. P. Perdew, M. Ernzerhof, and K. Burke, J. Chem. Phys. **105**, 9982 (1996).

[53] T. Lu and F. Chen, J. Comput. Chem. **33**, 580 (2012).

[54] A. D. Becke, Phys. Rev. A **38**, 3098 (1988).

[55] C. Adamo and V. Barone, J. Chem. Phys. **110**, 6158 (1999).

[56] J. Heyd, G. E. Scuseria, and M. Ernzerhof, J. Chem. Phys. **118**, 8207 (2003).

[57] M. A. Rohrdanz, K. M. Martins, and J. M. Herbert, J. Chem. Phys. **130**, 054112 (2009).

[58] J.-D. Chai and M. Head-Gordon, J. Chem. Phys. **128**, 084106 (2008).

[59] S. Goedecker, M. Teter, and J. Hutter, Phys. Rev. B **54**, 1703 (1996).

[60] J. Hutter, M. Iannuzzi, F. Schiffmann, and J. VandeVondele, Wiley Interdiscip. Rev. Comput. Mol. Sci. **4**, 15 (2013).

[61] E. F. Valeev, V. Coropceanu, D. A. da Silva Filho, S. Salman, and J.-L. Brédas, J. Am. Chem. Soc. **128**, 9882 (2006).

[62] M. Elstner and G. Seifert, Philos. Trans. R. Soc. A: Math. Phys. Eng. Sci. **372**, 20120483 (2014).

[63] M. Gaus, Q. Cui, and M. Elstner, WIREs Comput. Mol. Sci. **4**, 49 (2013).

[64] Y. Yang, H. Yu, D. York, M. Elstner, and Q. Cui, J. Chem. Theory Comput. **4**, 2067 (2008).

[65] S. Giannini, A. Carof, M. Ellis, H. Yang, O. G. Ziogos, S. Ghosh, and J. Blumberger, Nat. Commun. **10**, (2019).

[66] O. G. Ziogos, S. Giannini, M. Ellis, and J. Blumberger, J. Mater. Chem. C **8**, 1054 (2020).

[67] H. Sirringhaus, R. H. Friend, C. Wang, J. Leuninger, and K. Müllen, J. Mater. Chem. **9**, 2095 (1999).

[68] M. Mas-Torrent, M. Durkut, P. Hadley, X. Ribas, and C. Rovira, J. Am. Chem. Soc. **126**, 984 (2004).

[69] M. Mas-Torrent and C. Rovira, Chem. Soc. Rev. **37**, 827 (2008).

[70] P. Gao, D. Beckmann, H. N. Tsao, X. Feng, V. Enkelmann, W. Pisula, and K. Müllen, Chem. Commun. 1548 (2008).

[71] T.-F. Yang, S.-H. Huang, Y.-P. Chiu, B.-H. Chen, Y.-W. Shih, Y.-C. Chang, J.-Y. Yao, Y.-J. Lee, and M.-Y. Kuo, Chem. Commun. **51**, 13772 (2015).

[72] Z. Bao, A. J. Lovinger, and A. Dodabalapur, Adv. Mater. **9**, 42 (1997).

[73] A. Mahmood, J.-Y. Hu, B. Xiao, A. Tang, X. Wang, and E. Zhou, J. Mater. Chem. A **6**, 16769 (2018).

[74] Y. Sakamoto, T. Suzuki, M. Kobayashi, Y. Gao, Y. Fukai, Y. Inoue, F. Sato, and S. Tokito, J. Am. Chem. Soc. **126**, 8138 (2004).

[75] F. Würthner, C. R. Saha-Möller, B. Fimmel, S. Ogi, P. Leowanawat, and D. Schmidt, Chem. Rev. **116**, 962 (2015).

[76] R. K. Gupta and A. A. Sudhakar, Langmuir **35**, 2455 (2018).

[77] B. Wex, B. R. Kaafarani, K. Kirschbaum, and D. C. Neckers, J. Org. Chem. **70**, 4502 (2005).

[78] C. Mitsui, H. Tsuyama, R. Shikata, Y. Murata, H. Kuniyasu, M. Yamagishi, H. Ishii, A. Yamamoto, Y. Hirose, M. Yano, T. Takehara, T. Suzuki, H. Sato, A. Yamano, E. Fukuzaki, T. Watanabe, Y. Usami, J. Takeya, and T. Okamoto, J. Mater. Chem. C **5**, 1903 (2017).

[79] Q. Miao, T.-Q. Nguyen, T. Someya, G. B. Blanchet, and C. Nuckolls, J. Am. Chem. Soc. **125**, 10284 (2003).

[80] Y. Ma, Y. Sun, Y. Liu, J. Gao, S. Chen, X. Sun, W. Qiu, G. Yu, G. Cui, W. Hu, and D. Zhu, J. Mater. Chem. **15**, 4894 (2005).

[81] K. P. McKenna and J. Blumberger, Phys. Rev. B **86**, 245110 (2012).

[82] J. Blumberger and K. P. McKenna, Phys. Chem. Chem. Phys. **15**, 2184 (2013).

[83] N. Gillet, L. Berstis, X. Wu, F. Gajdos, A. Heck, A. de la Lande, J. Blumberger, and M. Elstner, J. Chem. Theory Comput. **12**, 4793 (2016).

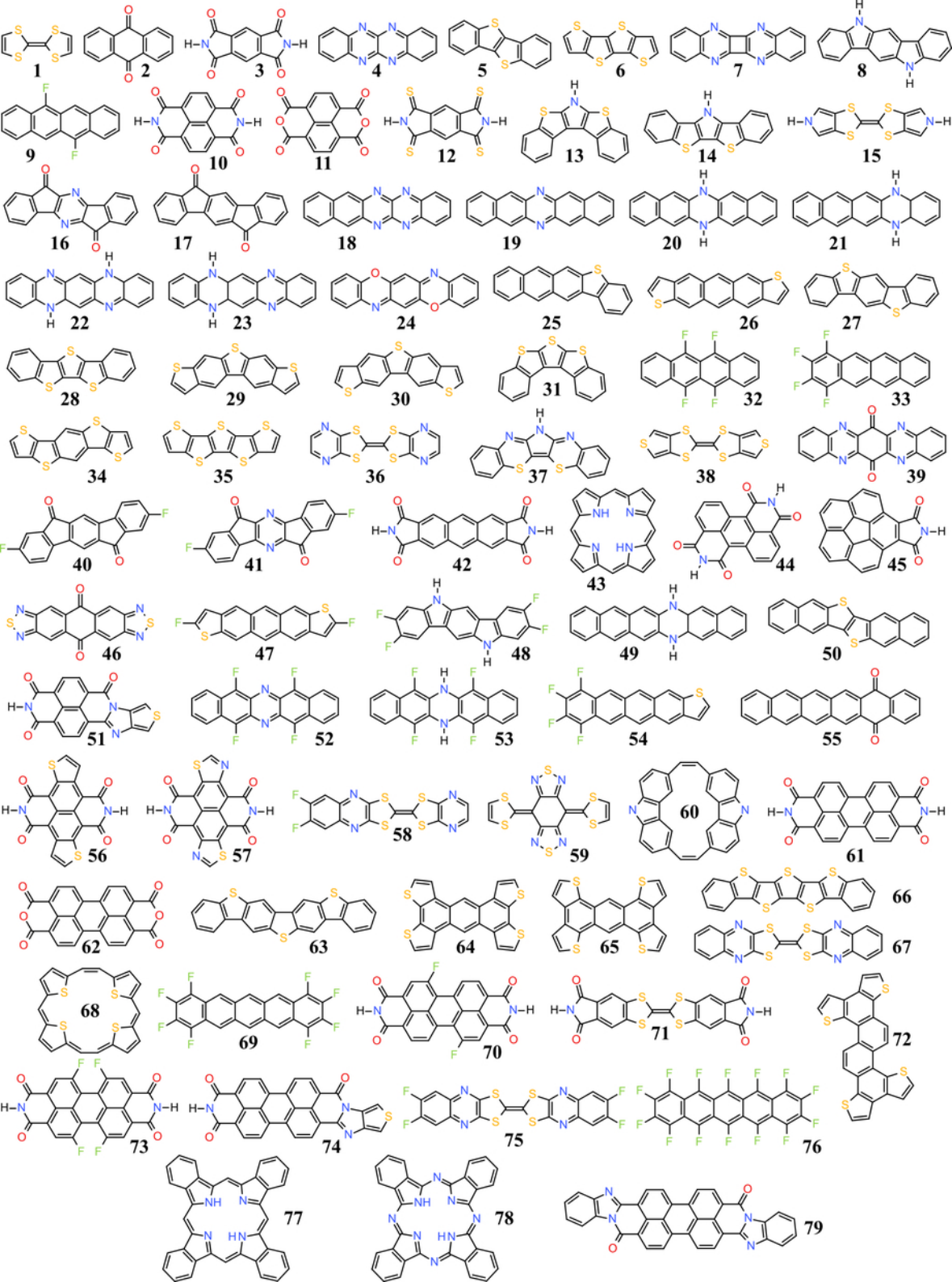
1
2
3
4
5
6
7
8
9
10
11
12
13
14
15
16
17
18
19
20
21
22
23
24
25
26
27
28
29
30
31
32
33
34
35
36
37
38
39
40
41
42
43
44
45
46
47
48
49
50
51
52
53
54
55
56
57
58
59
60
61
62
63
64
65
66
67
68
69
70
71
72
73
74
75
76
77
78
79

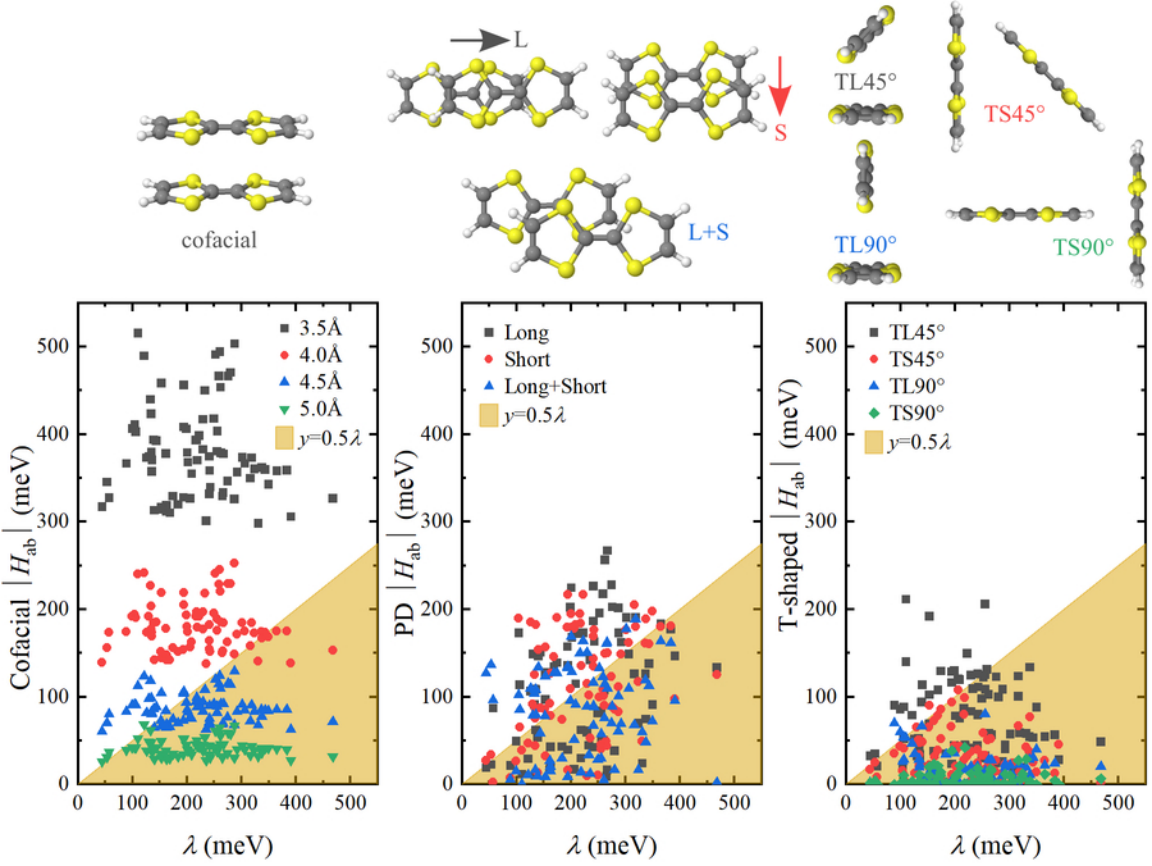
cofacial
L
S
L+S
TL45°
TS45°
TL90°
TS90°
3.5Å
4.0Å
4.5Å
5.0Å
y=0.5λ
Cofacial |H_ab| (meV)
λ (meV)
Long
Short
Long+Short
y=0.5λ
PD |H_ab| (meV)
λ (meV)
TL45°
TS45°
TL90°
TS90°
y=0.5λ
T-shaped |H_ab| (meV)
λ (meV)

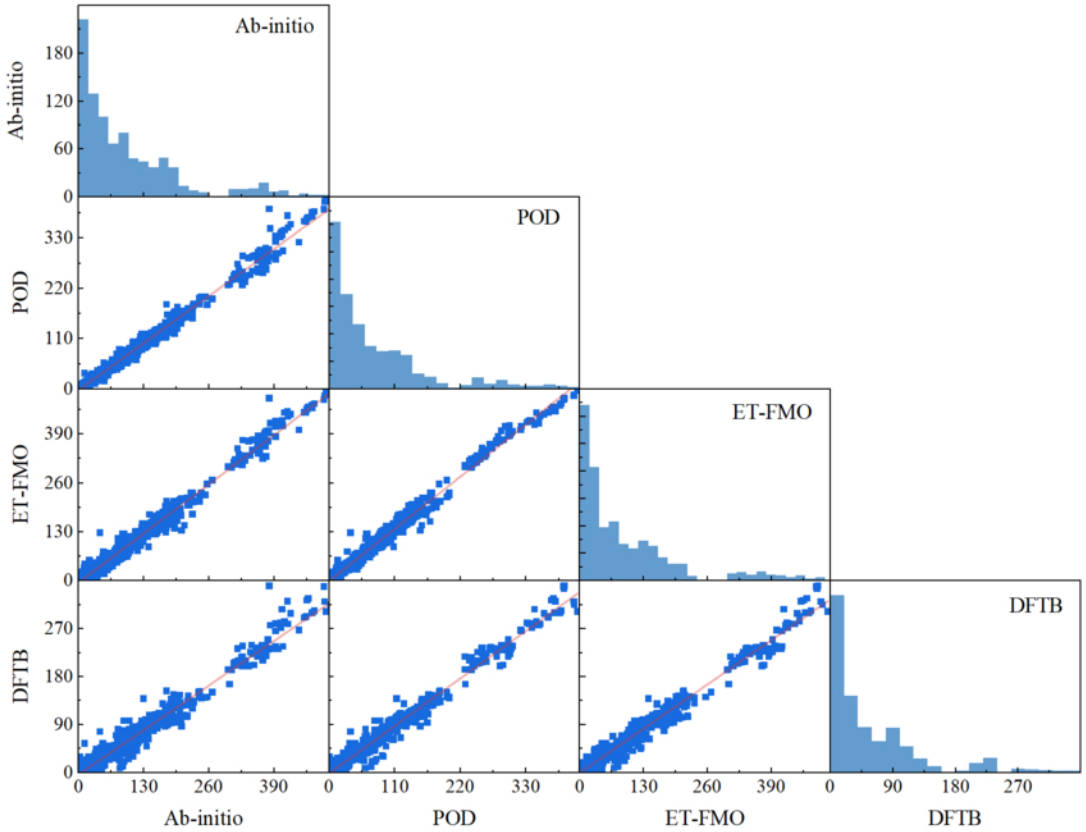
Ab-initio
POD
ET-FMO
DFTB
Ab-initio
POD
ET-FMO
DFTB
0
60
120
180
0
110
220
330
0
130
260
390
0
90
180
270
0
130
260
390
0
110
220
330
0
130
260
390
0
90
180
270

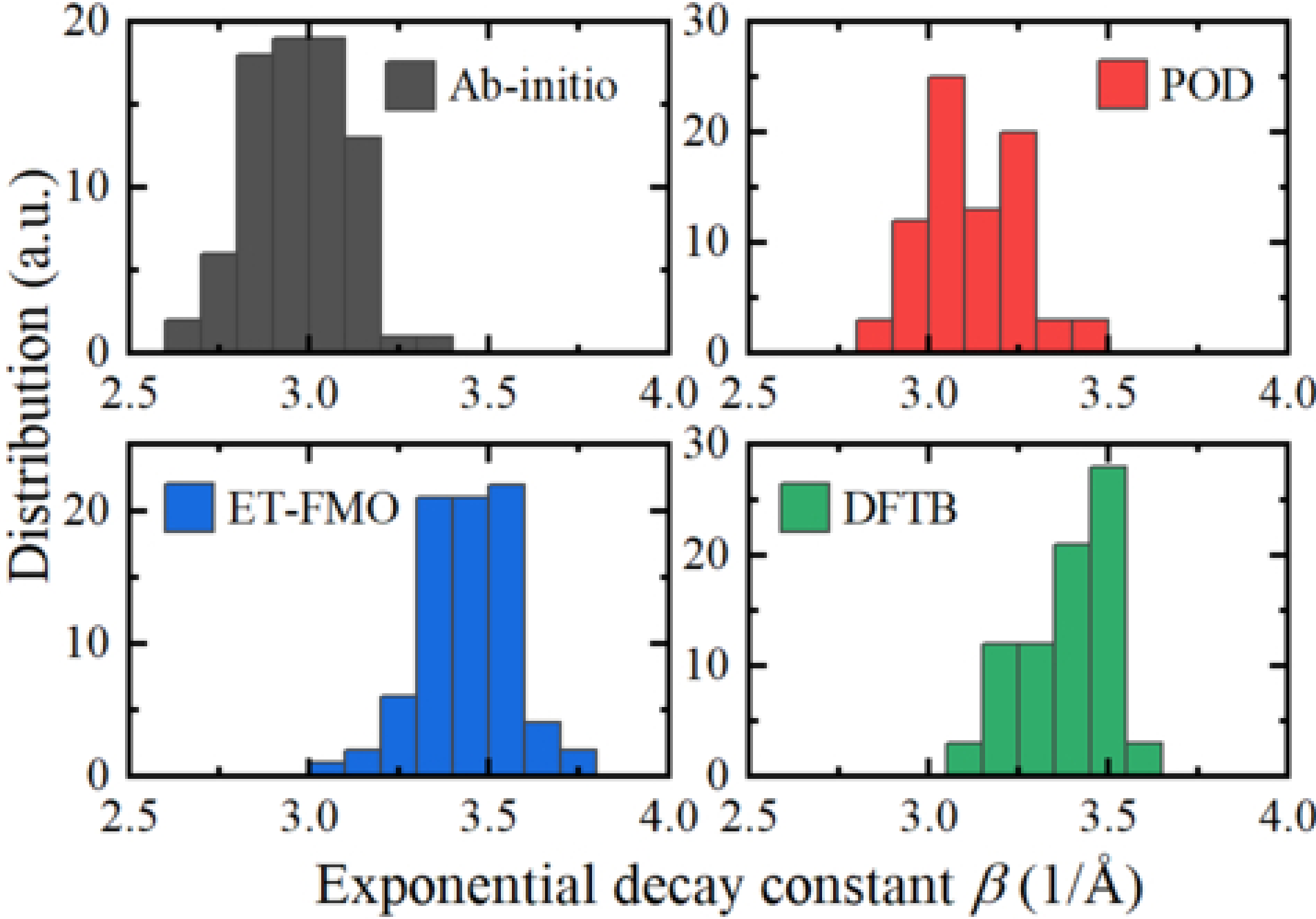
Ab-initio
POD
ET-FMO
DFTB
Distribution (a.u.)
Exponential decay constant β (1/Å)
0
10
20
30
2.5
3.0
3.5
4.0

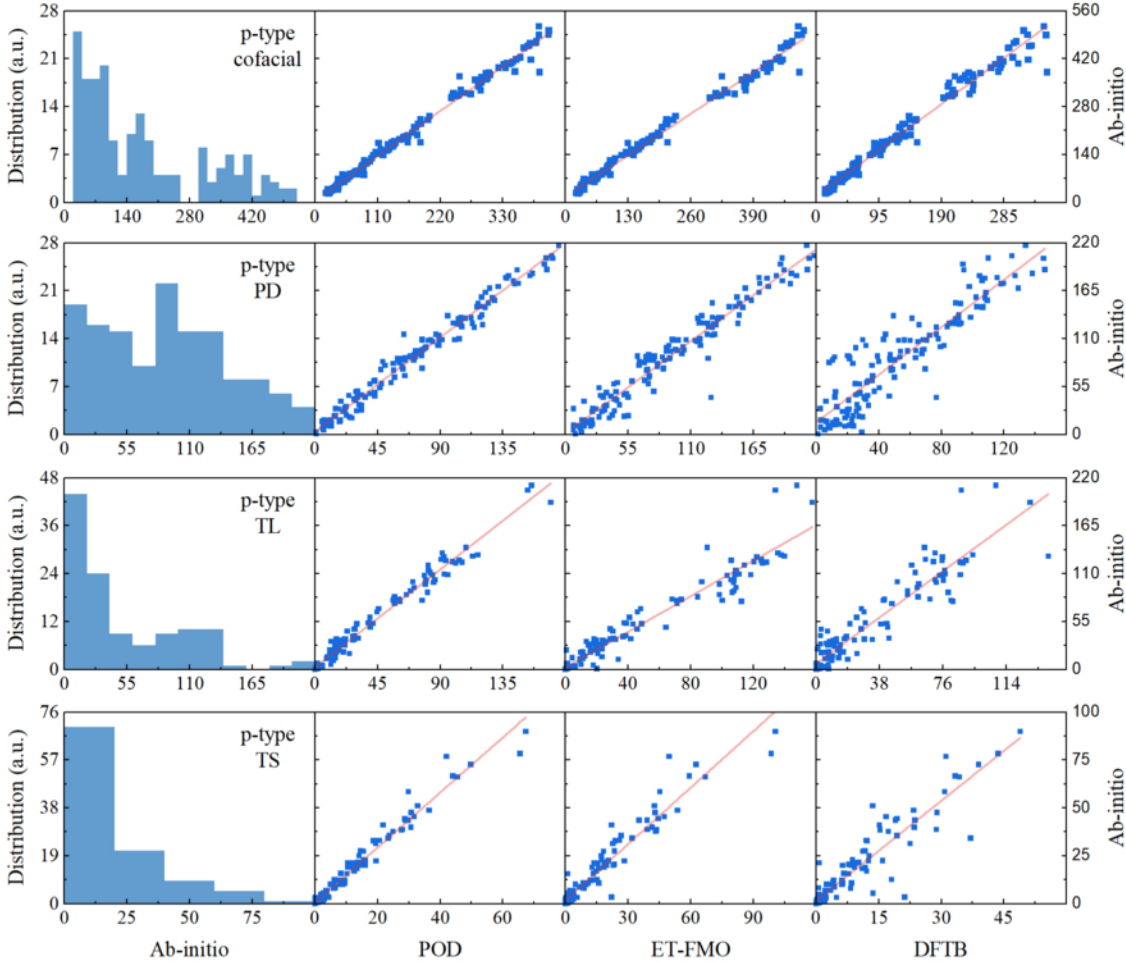
p-type
cofacial
p-type
PD
p-type
TL
p-type
TS
Distribution (a.u.)
Ab-initio
Ab-initio
POD
ET-FMO
DFTB

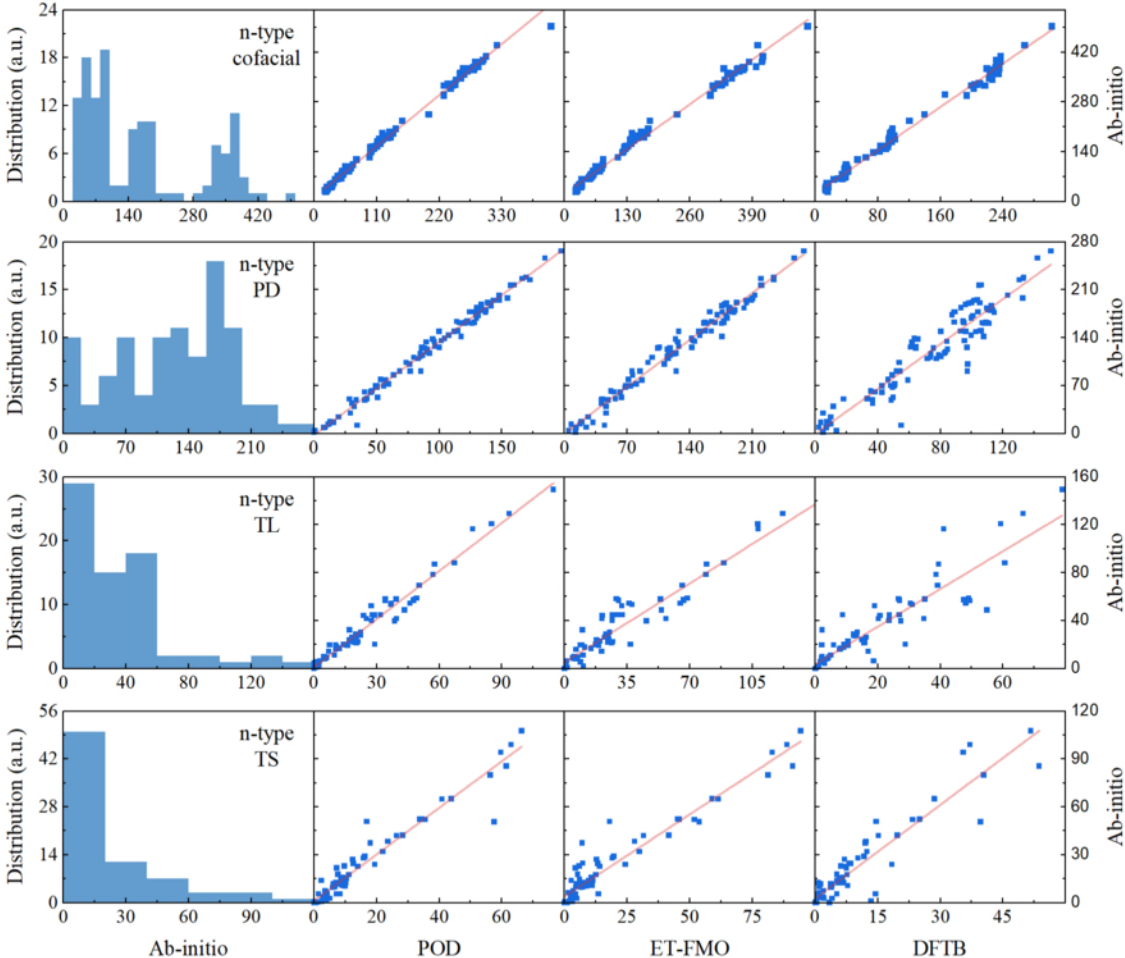
n-type
cofacial
n-type
PD
n-type
TL
n-type
TS
Distribution (a.u.)
Ab-initio
Ab-initio
POD
ET-FMO
DFTB